The Effect of Decoupled Low-Level Flow on Winter Orographic Clouds and Precipitation in the Yampa River Valley

THOMAS CARL PETERSON, L. O. GRANT, W. R. COTTON AND D. C. ROGERS

Atmospheric Science Department, Colorado State University, Fort Collins, Colorado

(Manuscript received 3 March 1990, in final form 23 August 1990)

ABSTRACT

Mountains often act as barriers to low-level flow creating regions of stagnant, decoupled flow within thermally stratified air masses. This paper addresses the question: how does a region of low-level decoupled flow affect the overlying orographic cloud?

Three different methodologies were used to examine this problem. The first method involved analysis of one and a half months of precipitation and wind data from a 24-station mesonetwork located in the Yampa River valley and surrounding mountains of northwest Colorado during the winter of 1981/1982 as part of the third Colorado Orographic Seeding Experiment (COSE III). The second method was a case study analysis of two orographic storms using data from an instrumented cloud physics aircraft to supplement the data from the mesonetwork. The third method involved two-dimensional numerical simulations using Colorado State University's Regional Atmospheric Modeling System (RAMS).

The results show that the presence of extensive low-level decoupled flow causes part of the orographic lift of the mountain barrier to be experienced upstream of the barrier. This changes the location of condensate production which in turn shifts precipitation upstream and appears to enhance the precipitation efficiency for the entire barrier.

1. Introduction

During winter orographic storms, the surface layer upwind of the barrier can flow up and over the barrier, it can be blocked and stagnant, it can flow parallel to the mountain barrier, or it can even flow back upstream 180 degrees with respect to the ridge-top winds. When the low-level air is not flowing over the barrier with the synoptic-scale winds, the low-level flow can be considered decoupled from the free atmosphere.

The physics involved in the creation of low-level decoupled flow can vary. For instance, radiative cooling of the surface air on the mountainsides produces a shallow layer of cold, dense air, which flows down valley in what is commonly called drainage flow. Another process for creating low-level blocked flow is the cooling of stably stratified incoming flow as it experiences adiabatic ascent. This creates a positive pressure perturbation and a negative pressure gradient directed upstream of the barrier. This can slow the oncoming flow or even produce down-valley flow.

Many researchers have studied low-level decoupled flow in terms of blocking by the barrier or in terms of mountain/valley circulations. However, we know of only three other detailed studies of the effect of low-level decoupled flow on precipitation. These studies indicate that there are changes in precipitation intensity and location due to differing decoupled flows, but they do not agree on what the changes are. Grossman and Durran (1984) indicate that low-level blocking upstream of a mountain barrier causes rising of air far upwind of the barrier resulting in precipitation upstream of the barrier. Smolarkiewicz et al. (1988) are more specific, indicating that it is the Froude number ($\mathrm{Fr} = U/Nh$) that exerts primary control over the location and strength of the convergence zone, and hence cloud band, upwind of the island of Hawaii. Increasing the Froude number trends to induce a stronger band that forms closer to the shore. Marwitz (1980), however, interprets the effect of low-level blocking quite differently. He suggests that upstream blocking acts to decrease the effective height of the barrier. Decreasing the effective height of the barrier decreases orographic precipitation.

The working hypothesis used during this research is that low-level decoupled flow does not decrease the effective height of the barrier, but rather acts as an extension of the mountain for orographic lift purposes, see Figs. 1a,b. If the effective shape of the mountain barrier was changed suddenly by decoupled low-level flow, the location and intensity of orographic lift would change, the location of precipitation would change, and perhaps even precipitation efficiency could change drastically. Understanding such effects could be important to precipitation forecasts in mountainous areas

Corresponding author address: Mr. Thomas Carl Peterson, Dept. of Atmospheric Science, Colorado State University, Fort Collins, CO 80523.

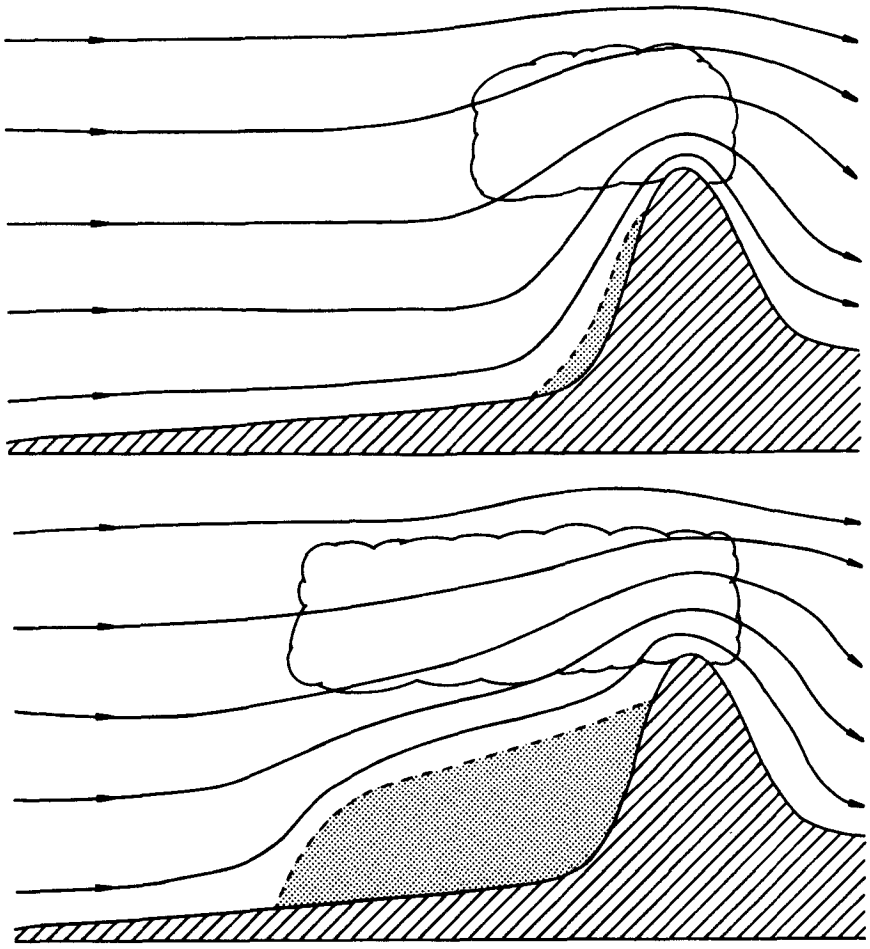

FIG. 1. Conceptual model for the working hypothesis that low-level decoupled flow (stippled area) acts as an extension of the mountain barrier for orographic lift purposes which would then alter the location of condensate production and hence precipitation. A small amount of decoupled low-level flow (a) allows parcel lift to occur near the barrier while a large amount of low-level decoupled flow (b) forces parcel lift to occur upstream of the barrier.

and determining the design of seeding experiments and evaluation of their results.

2. Approach to the problem

The research presented here examines the effect that low-level decoupled flow has on the overlying winter orographic clouds. Three methods were used in this analysis. The first method took a climatological approach by examining one and a half months of precipitation and wind data from a mesonetwork to see how precipitation intensity and location varied with the extent of decoupled flow upwind of the barrier. The second method involved two case study analyses that used data from an instrumented aircraft to examine cloud conditions when both the extent of low-level decoupled flow upwind of the barrier was small and when it was large. The third method used numerical simulations of orographic clouds with conditions that produced two very different patterns of low-level decoupled flows.

3. Data sources

The data used in this research were collected during the third Colorado Orographic Seeding Experiment (COSE III) (Rauber and Grant 1982) during the winter of 1981/82. COSE III was a large multipurpose experiment located near Steamboat Springs, Colorado. The topography of the COSE III research area is shown in Fig. 2. The four prime topographic features of this area are:

(i) The Yampa River valley which runs almost due west.

(ii) The valley sides that increase in height towards the east.

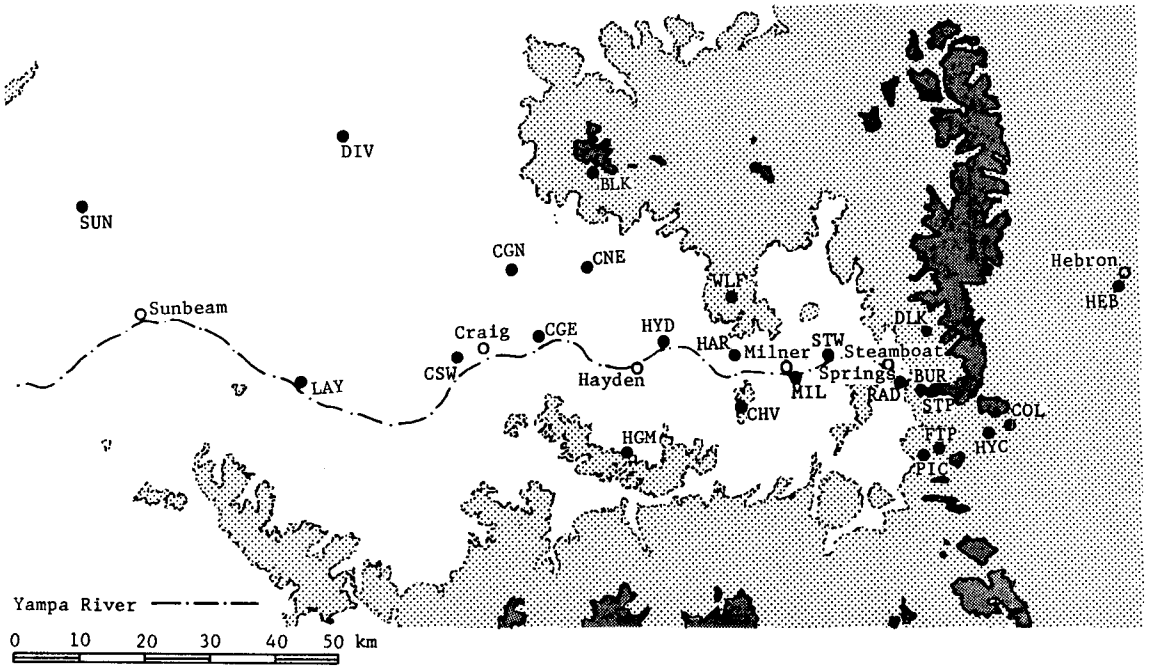

FIG. 2. A map of the COSE III research area showing towns (open circles) and PROBE stations (closed circles). Lightly stippled area represents elevations between 2286 m (7500 ft) and 3048 m (10 000 ft) MSL. Darker stippling represents elevations greater than 3048 m MSL. Dot–dash line indicates the Yampa River.

(iii) The sharp rise of the Park Range which runs almost due north/south and blocks the east end of the valley.

(iv) Many smaller mountains and hills are present in the valley. Notable among these are Quarry Mountain southwest of Steamboat Springs and the ridges that form a constriction in the valley west of Milner.

COSE III instrumentation included Ku-band radar, rawinsondes released every 3 h during storm events upstream at Craig and downstream at Hebron (see Fig. 2), and the Bureau of Reclamation's mesonetwork called the Portable Remote Observation Equipment (PROBE). The PROBE network consisted of 24 stations that reported temperature, pressure, relative humidity, wind speed and direction, and precipitation accumulation every 15 min. The PROBE stations were located in the Yampa River valley, across the Park Range Continental Divide and down the east side of the Park Range. They cover an area with an east–west length of 160 km and a north–south extent of about 50 km. The locations of PROBE stations are indicated by solid dots in Fig. 2. The PROBE stations covered a wide range of elevations from 1884 to 3149 m MSL.

In addition to ground-based sensing, Colorado International Corporation provided a Cheyenne aircraft with cloud physics instrumentation including Particle Measuring Systems' forward scattering spectrometer probe (FSSP) and Particle Measuring Systems' two-dimensional cloud spectrometer (Hobbs and Deepak 1981). Liquid water was calculated from the FSSP which has a droplet-size range from 2–45 μm with a resolution of 0.5–3 μm and a concentration range of 0.1–10 000 cm^{-3}. Ice-crystal size and concentration was determined from the 2D cloud spectrometer which has a size range of 37.5–1200 μm with a resolution of 37.5 μm and a concentration range of 0.1–10 000 l^{-1}.

4. Analyses

a. Method 1: Climatological approach

One cloud physics related parameter recorded at all 24 PROBE stations 24-hours-a-day was precipitation. This section presents results of an investigation of precipitation intensity and location and how they vary depending on the magnitude of low-level decoupled flow based on PROBE precipitation data. This analysis takes a climatological approach by analyzing all the PROBE data collected during the winter of 1981/82.

If the low-level flow is not directed over the barrier with the synoptic-scale winds, it is decoupled from the synoptic-scale winds. However, to be accurate in determining what could be considered decoupled flow, the dataset would have to include near-continuous soundings to determine when the flow is decoupled. Such data is not available. Therefore, for purposes of this analysis, surface PROBE mesonet wind data were used to show the decoupling of the low-level flows from the synoptic-scale flow at and above mountaintop level

by choosing a threshold value for the cross-barrier component of the wind to specify the decoupled flow. Lee (1981) used the value of 2.0 m s^{-1} for the cross-barrier component to be the cutoff point for decoupled flow and Graw (1990) used 1.0 m s^{-1} for the threshold.

For the research presented here, a 1.5 m s^{-1} surface cross-barrier wind threshold value for determining low-level decoupled flow was applied to two valley-floor stations. First it was applied to station MIL (see Fig. 2) at the lower end of the upper valley. Since the mountain barrier runs essentially north–south and the valley runs east–west, the u component of the wind was considered the cross-barrier wind and therefore used in evaluating if and how strongly the low-level air is moving over the barrier. If MIL's u wind (cross-barrier wind) was greater than 1.5 m s^{-1}, decoupled flow was determined to be either nonexistent or confined to the upper valley. Next the u wind at station CSW at the lower end of the middle valley was examined. If MIL's u wind was less than or equal to 1.5 m s^{-1} and CSW's u wind was greater than 1.5 m s^{-1}, the extent of decoupled flow was determined to extend to the middle valley. If both MIL's and CSW's u winds were less than or equal to 1.5 m s^{-1}, low-level decoupled flow was determined to extend into the lower valley.

For the climatological type analysis presented here, hourly PROBE data for the months of December 1981 and January 1982 were used. Since the focus of this research is on the effect of decoupled flow on clouds, the actual dataset used was limited to the hours when precipitation was reported somewhere in the PROBE network. During COSE III, there were 708 h with precipitation and wind data from the PROBE network. During these 708 h, decoupled flow was nonexistent or limited to the upper valley during 206 h, it extended into the middle valley during 230 h, and it reached all the way to the lower valley for 272 h.

An analysis involving the depth of low-level decoupled flow has been used in the case study analyses. However, for purposes of the climatological analysis of two months of PROBE data presented here, the depth of low-level decoupled flow was not considered. Only the westward extent of low-level decoupled flow as determined by two valley-floor stations was used in this analysis.

For analysis of precipitation, the PROBE stations were divided into five groups based on station location. Three stations were in the over-the-barrier group (OB), five stations were on-the-barrier (B), and four each were in the upper valley (UV), middle valley (MV), lower valley (LV), and valley sides (VS) as shown in Figs. 3 and 4. A station with an hour of missing precipitation data was assumed to have received the average precipitation reported by its group for that hour.

The lightest average precipitation occurred when blocked flow stretched all the way into the lower valley. This was primarily due to the total lack of intense precipitation during times of extensive blocked flow. For example, the maximum precipitation intensity averaged for all 24 PROBE stations for when decoupled flow was nonexistent or limited to the upper valley or when it was in the middle valley was greater than 1.4 mm h^{-1}, which is an order of magnitude greater than the 0.12 mm h^{-1} maximum recorded when decoupled flow extended to the lower valley.

In order to look at the change in location of precipitation, the percent of precipitation on a per station basis is plotted by location in Fig. 5. In order for precipitation to be registered in the hand-corrected hourly precipitation records for COSE III, a threshold value of 3 mm of water equivalent must be reached. When the precipitation was very light, this threshold makes comparing precipitation from one location to another less accurate. Therefore, only data for those hours when decoupled flow was in the upper valley (which includes hours when decoupled flow was nonexistent) or middle valley were plotted in Fig. 5.

The observed changes in precipitation location shown in Fig. 5 were basically a westward shift in precipitation corresponding to a westward increase in decoupled flow. This could be interpreted as supporting Grossman and Durran's (1984) conclusion that low-level blocking causes lift upstream of the barrier. This aspect of the relationship between the extent of decoupled low-level flow and precipitation seems to be causal, with the magnitude of decoupled flow altering the location of precipitation by altering the location of orographic lift as air is forced to rise over the layer of decoupled air as well as the mountain. If the low-level decoupled flow extends 60 km upwind of the barrier, then the orographic lift would initially be experienced 60 km farther upwind as the oncoming air rises over the stable decoupled flow. The location of precipitation in mountainous regions is directly related to orographic lift. Therefore, starting the mountain's orographic lift farther upstream would shift precipitation upstream since ice crystals would have a longer time to grow and fall, and in convectively unstable situations, convection could be initiated farther upstream.

The observed decrease in precipitation intensity with increased decoupled flow could be interpreted as supporting Marwitz's (1980) conclusion that blocked flow decreases the effective height of the barrier. However, Grossman and Durran's conclusion is in conflict with Marwitz's conclusions; Grossman and Durran propose that low-level blocked flow causes lift while Marwitz suggests that blocked flow reduces lift. Clearly another explanation for the observed change in precipitation intensity is needed. As noted previously, decoupled low-level flow can be created by dynamic blocking of oncoming flow or by radiatively inducing drainage flows. While a theoretical framework relating the magnitude of radiatively induced drainage flows with precipitation intensity is not clear, a connection between dynamic blocking and precipitation intensity can be formulated.

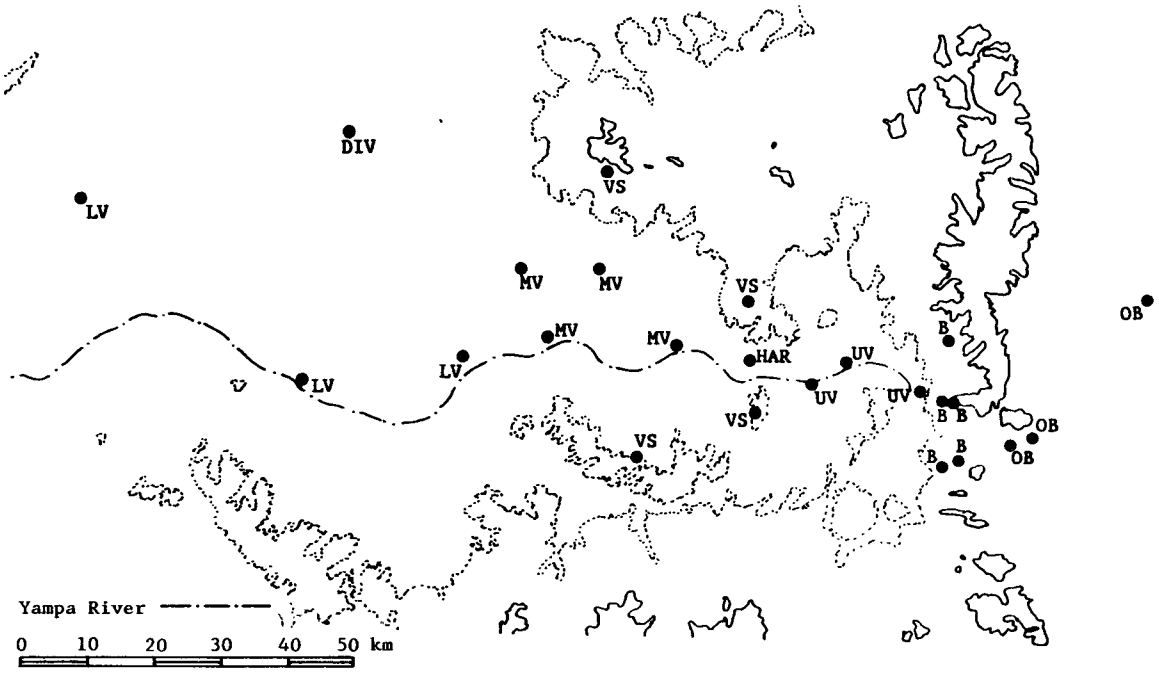

FIG. 3. Map of the COSE III research area showing PROBE station precipitation groups: OB for over-the-barrier, B for barrier, UV for upper valley, MV for middle valley, LV for lower valley, VS for valley sides, and two individual stations HAR and DIV.

Pierrehumbert and Wyman (1985) showed that in the nonrotating case (which may be most applicable in the cases of modest degree of blocked flow due to the effect of the valley sides), the Froude number is the "sole parameter" controlling blocking of oncoming flow. The Froude number is $\mathrm{Fr} = U/Nh$, where U is the speed of the oncoming flow, N is the Brunt–Väisälä frequency, $N^2 = (g/\theta)(d\theta/dz)$ and h the maximum

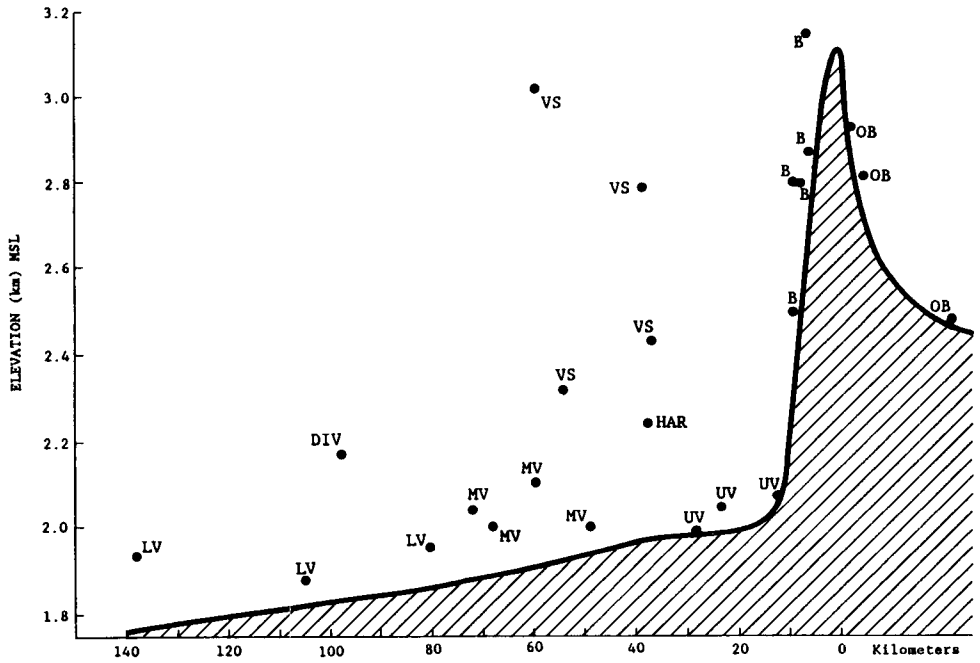

FIG. 4. The X–Z cross section of the COSE III research area showing the same PROBE station precipitation groups shown in Fig. 3. The valley-floor level shown is the level of the Yampa River at that distance from the barrier crest.

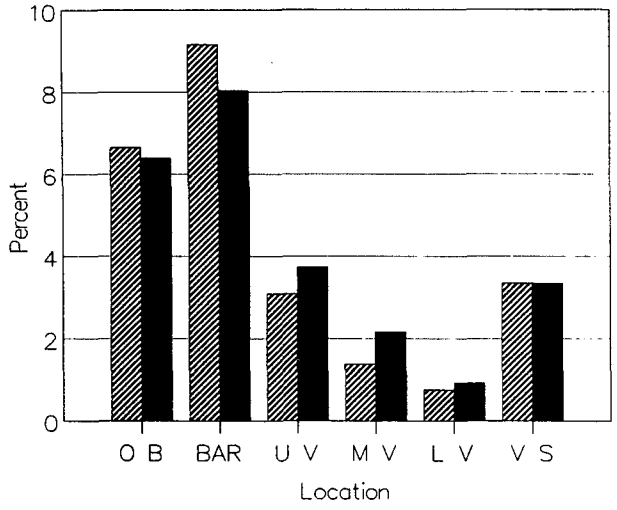

FIG. 5. Percent of precipitation by location on a per station average. Striped bar represents hours when decoupled flow was nonexistent or limited to the upper valley. Solid bar represents hours when the western end of low-level decoupled flow was determined to be in the middle valley. Locations are over-the-barrier (OB), on the barrier (B), upper valley (UV), middle valley (MV), lower valley (LV), and valley sides (VS).

mountain height. The Froude number represents the square root of the ratio of the kinetic energy in the horizontal flow over the energy required to lift a parcel of air from the surface to mountain top height through the stably stratified environment. Therefore, for a given atmospheric stability, the degree of blocked flow tends to be small when cross-barrier winds are strong, and large when cross-barrier winds are weak. It is hypothesized that this link is generally applicable for the storm events studied.

Orographic clouds have been likened to cumulus clouds turned on their sides with the cross-barrier flow feeding in moisture much the way the updraft does in cumulus clouds. Therefore, for a given atmospheric humidity, strong cross-barrier winds will produce more condensate per hour in an orographic cloud than weak cross-barrier winds. This is a prime factor in increased precipitation, although just having more condensate form per hour does not guarantee that more precipitation will reach the ground. Also, when cross-barrier winds are weak and less condensate forms, orographic precipitation can be expected to be light.

Therefore, the decrease in precipitation intensity with increasing extent of decoupled low-level flow can be explained by the fact that strong cross-barrier winds increase precipitation intensity and decrease the extent of low-level decoupled flow. However, since the location of parcel lift could not be determined by this climatological approach, this proposed explanation for the observed changes in precipitation intensity suggests a similar explanation for the observed changes in precipitation location: the strong cross-barrier winds that increase precipitation intensity and decrease the extent of low-level flow simply blow the crystals farther downstream than the weak cross-barrier winds associated with large areas of decoupled low-level flow.

b. Method 2: Case studies

The primary purpose of this case study analysis is to determine the location of orographic lift experienced by parcels moving through the orographic clouds over a small area of decoupled flow and a large area of decoupled flow. The storms on 16 and 23 January 1982 were shallow, 1–1.5 km thick, orographic cloud systems; a type of storm system that frequently forms in northern Colorado as a result of a strong cross-barrier flow accompanied by midlevel moisture advected in from the west.

Both storms had similar synoptic conditions. Surface weather maps for both 16 and 23 January 1982 show a stationary front near the research area running in a generally north to south direction stretching from Canada to Texas. The 700-hPa maps shown in Figs. 6a,b indicate advection of moisture from the west. Table 1 shows that winds at midcloud levels were basically perpendicular to the barrier and parallel with the valley, with the 16 January winds being weaker than the 24 January winds. Both cases had thermally stable soundings; see Figs. 7a,b with inversions at the 550-hPa level.

The Froude number calculated from the sounding taken 1900 UTC 16 January 1982 was 1.43. For the 23–24 January 1982 storm, Fr = 1.09 at 2100 UTC and Fr = 0.94 at 0000 UTC 24 January. So despite 23 January having a greater cross-barrier wind than 16 January, the Froude number is lower and the length of decoupled flow is greater on 23–24 January than 16 January.

The winds recorded by the PROBE stations at the time of the analyzed flight through the cloud are shown in Figs. 8a,b. Note the contrast in the middle part of the Yampa Valley where the 16 January winds are up valley and the 23 January winds are down valley. This can also be seen clearly on the cross sections of the Yampa Valley in Figs. 9a,b. In the region 50–100 km west of the Continental Divide, the 16 January winds are blowing strongly up-valley while the approximate 1.5 m s^{-1} contour on the 23 January cross section is hundreds of meters above the floor of the Yampa Valley. Analysis of the extent of low-level decoupled flow during the 12 h of the 16 January storm and 9 h of the 23 January storm, showed that the extent of decoupled flow indicated in Figs. 8 and 9 are representative of the entire storms.

An analysis of crystal observations indicates that precipitation from both storms consisted primarily of dendrites with some aggregation and light riming. The 16 January storm produced more precipitation per hour than did the 23 January storm. Table 2 shows a comparison of the precipitation intensity of both storms at several locations. To more clearly see the differences

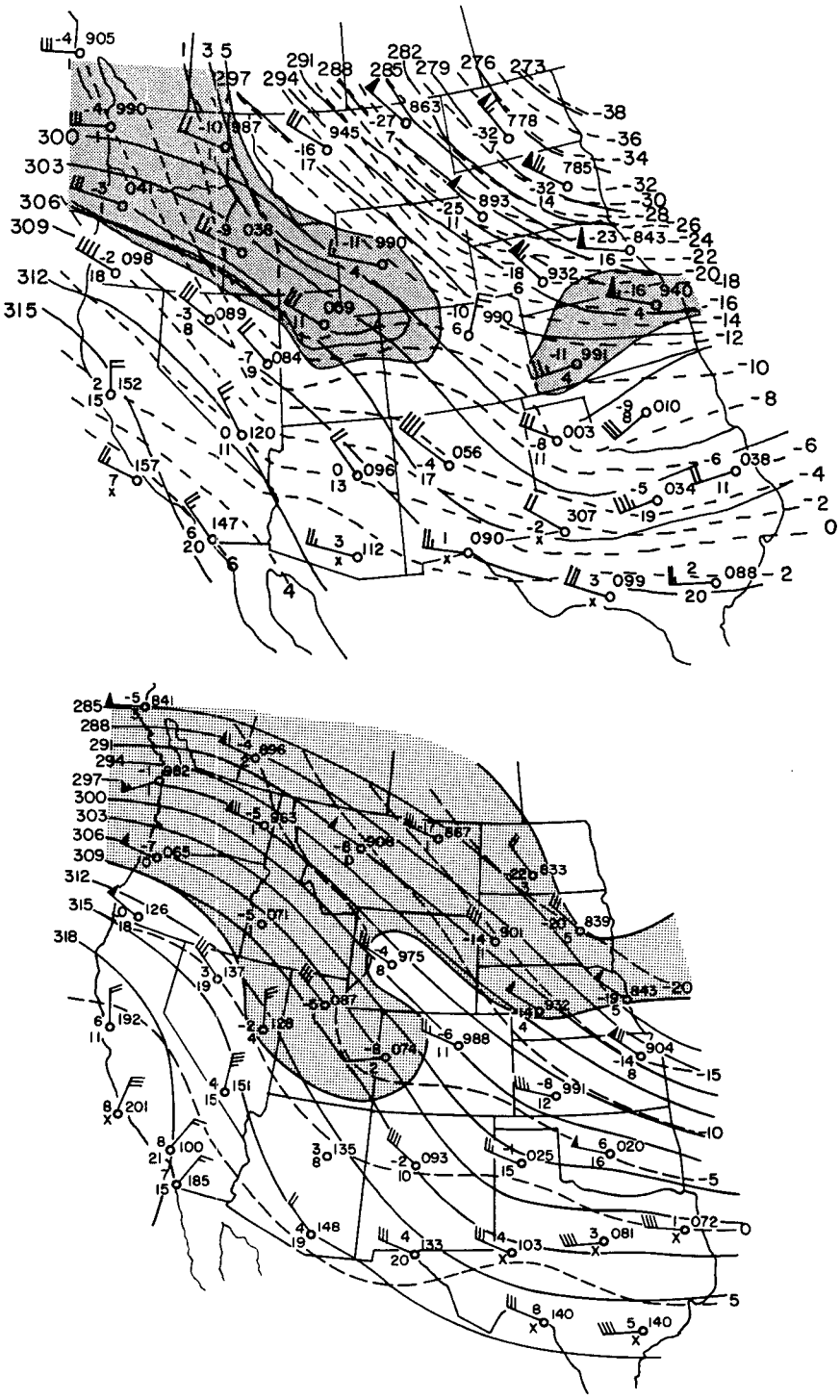

FIG. 6. (a) The 700-hPa analysis of height, temperature, and dewpoint depression ($T - T_d$) fields at 1200 UTC 16 January 1982. The shaded area denotes regions where ($T - T_d$) < 5°C. Long wind barbs are 5 m s^{-1}; pennant barbs are 25 m s^{-1}; from Rauber (1987). (b) The 700-hPa analysis for 0000 UTC 24 January 1982. See (a) for data format.

in precipitation during the two storms, Fig. 10 shows a comparison of the percent of precipitation falling on the various station groups. The 16 January storm snowed heaviest on the eastern edge of the research area, decreasing in intensity to the west, with no precipitation falling in the middle or lower valley. A pre-

TABLE 1. Midcloud-level winds taken from soundings 70 km upwind of the barrier crest at Craig, Colorado.

	16 January 1982		23 January 1982	
Height (m MSL)	Direction (°)	Speed (m s^{-1})	Direction (°)	Speed (m s^{-1})
3658	275	13.9	285	24.7

cipitation maximum on the barrier occurred on 23 January and a greater percentage of precipitation fell in the upper valley than 16 January, and some precipitation fell in the middle and lower valley.

Cloud conditions during these storms were measured by an instrumented aircraft. The aircraft flew near cloud top at 625 hPa and 3900 m MSL. Figures 11a,b show four relevant parameters from one pass through the cloud during each storm. On the bottom of Figs. 11a,b is the topography over which they flew. Though the aircraft attempted to fly the same path on both days, slight variations off the intended route lead to differences in the underlying topography.

On the top of Figs. 11a,b is the ice-crystal concentration determined from the 2D probe. Ice-crystal concentrations were much higher on 23 January than 16 January. Also, 23 January ice-crystal concentrations remained high over a large region from 30 km upwind of the barrier to 5 km downwind. Ice crystals observed on 16 January, on the other hand, had three small regions of moderate ice-crystal concentrations, two located over areas where the topography is increasing in height and one in the lee wave cloud.

Second from the top in Figs. 11a,b is the FSSP liquid-water content corrected for airspeed using the technique described in Cerni (1983). Immediately apparent are the facts that the aircraft did not pass out of the cloud on the upwind side on 23 January and that the liquid-water content is much higher on 23 January than 16 January. Also, there is a marked decrease in LWC on 23 January at 40–45 km upstream of the Continental Divide.

The third feature on Figs. 11a,b is the calculated parcel lift. The instrumented aircraft was not able to measure vertical wind velocity accurately enough for the upper region of an orographic cloud, so parcel lift was inferred based on the following assumptions.

- Steady-state conditions exist for the duration of the flight and for the time it takes a parcel to pass through the research area. (Ku-band radar shows little

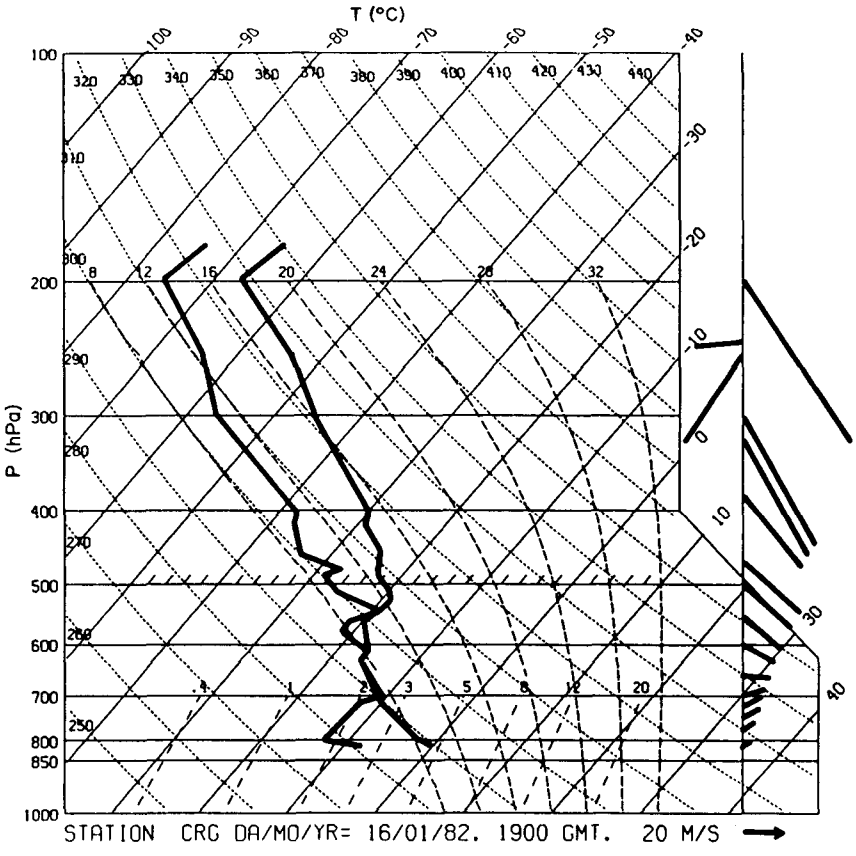

FIG. 7a. Sounding from rawinsonde taken 70 km upwind of the barrier crest at Craig, Colorado, 1900 UTC 16 January 1982. Wind vectors are shown on the right.

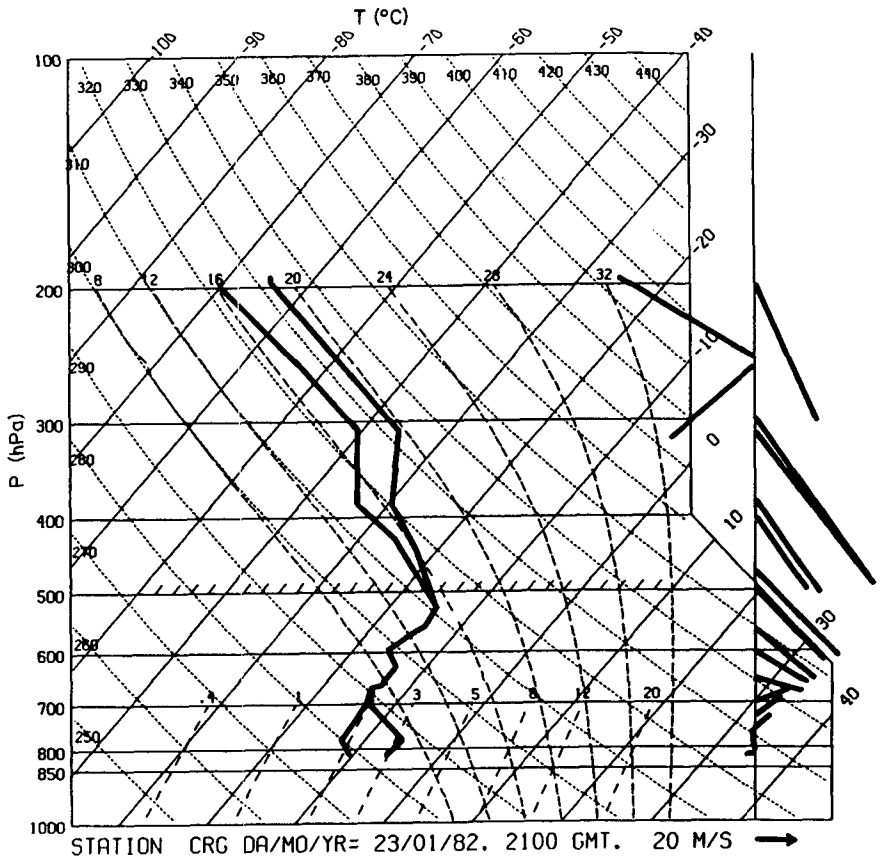

FIG. 7b. Sounding from rawinsonde taken 70 km upwind of the barrier crest at Craig, Colorado, 2100 UTC 23 January 1982. Wind vectors are shown on the right.

change during these time spans which supports this steady-state assumption.)

- Horizontal homogeneity in the north/south direction. (Since winds at flight level and flight path were both basically west/east, the influence of north/south inhomogeneity would be small, so this is a fairly realistic assumption to make.)
- Ice-crystal concentrations and size distributions observed by the aircraft are valid for the entire parcel.
- A very large parcel is considered which is 300 m high and 5 s of aircraft travel time horizontally.

These assumptions are consistent with the premise that the aircraft is essentially observing an evolving parcel. However, since the aircraft remains at the same altitude while the parcel is being lifted over the barrier, the aircraft must be moving farther down into this 300-m deep parcel.

As the parcel rises, it produces more liquid water. However, some of this liquid water would be depleted by ice-crystal growth. Therefore, to determine the liquid water that would be produced by parcel rise and from that the actual rise in the parcel, the amount of water depleted by ice-crystal growth must be determined. Ice-crystal growth rate depends on temperature, pressure, supersaturation, liquid-water content, and size of the ice crystal. To calculate ice-crystal growth rate as a function of crystal size at the temperature, pressure, and LWC of the parcels, modifications were made to the ice-crystal growth model of Rogers and Vali (1987).

Next, the ice-crystal concentrations were subdivided into as many as five different size bins. The same filter shown on total ice-crystal concentration and liquid-water content in Figs. 11a,b was applied to the different ice-crystal sizes. Since mass growth rate of the ice crystal increases with increasing size of crystal, the rate of liquid-water removal by ice-crystal growth was determined by using appropriate numbers from the crystal growth model for each size of crystal. These numbers changed every five seconds of aircraft time, but were applied for the appropriate interval of parcel time.

Adding filtered cloud liquid-water content to accumulated liquid-water equivalence removed by ice-crystal growth yields the accumulated liquid-water equivalent produced by parcel lift. The next step was a straightforward determination of how much lift would be required to produce a given accumulated liquid water equivalent at case study temperatures and pressures. The result, plotted third from the top in Figs. 11a,b, is parcel lift. This is how far the parcel would

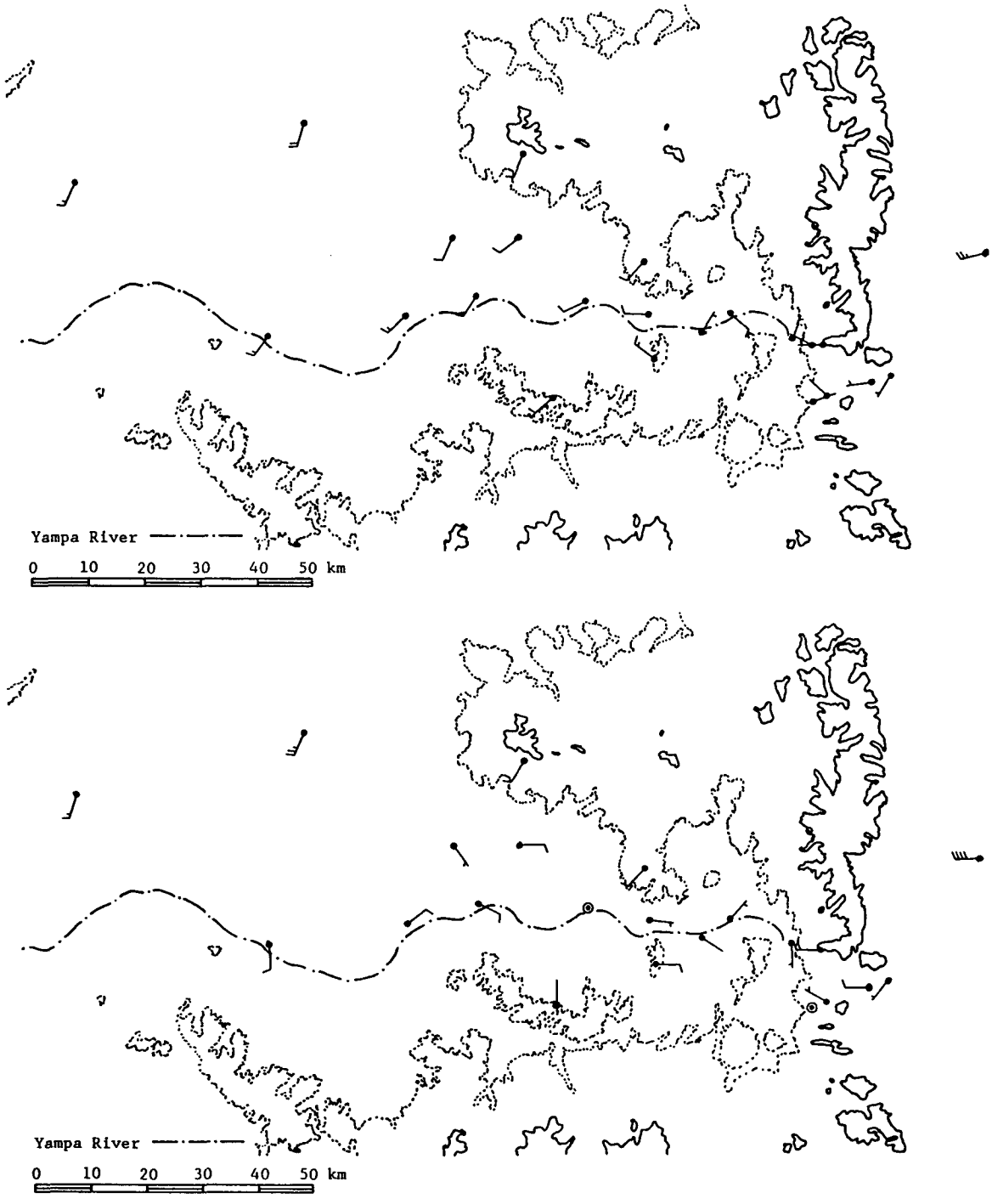

FIG. 8. Surface winds from PROBE stations recorded during aircraft flight time, 1930 UTC 16 January 1982. The long barbs are 5 m s^{-1}. The dashed line is the 2286-m MSL contour and the solid line is the 3048-m MSL contour. (b) Surface winds from PROBE stations recorded during aircraft flight time, 2245 UTC 23 January 1982. Long barbs are 5 m s^{-1}. The dashed line is the 2286-m MSL contour and the solid line is the 3048-m MSL contour.

have to rise to produce the calculated accumulated liquid-water equivalent.

Due to the many assumptions necessary to infer parcel lift from this technique, this technique is probably not accurate enough to reliably estimate vertical velocities. However, it should be accurate enough to determine the general regions of parcel lift. For 16 January, the result shown in Fig. 11a indicates that parcel

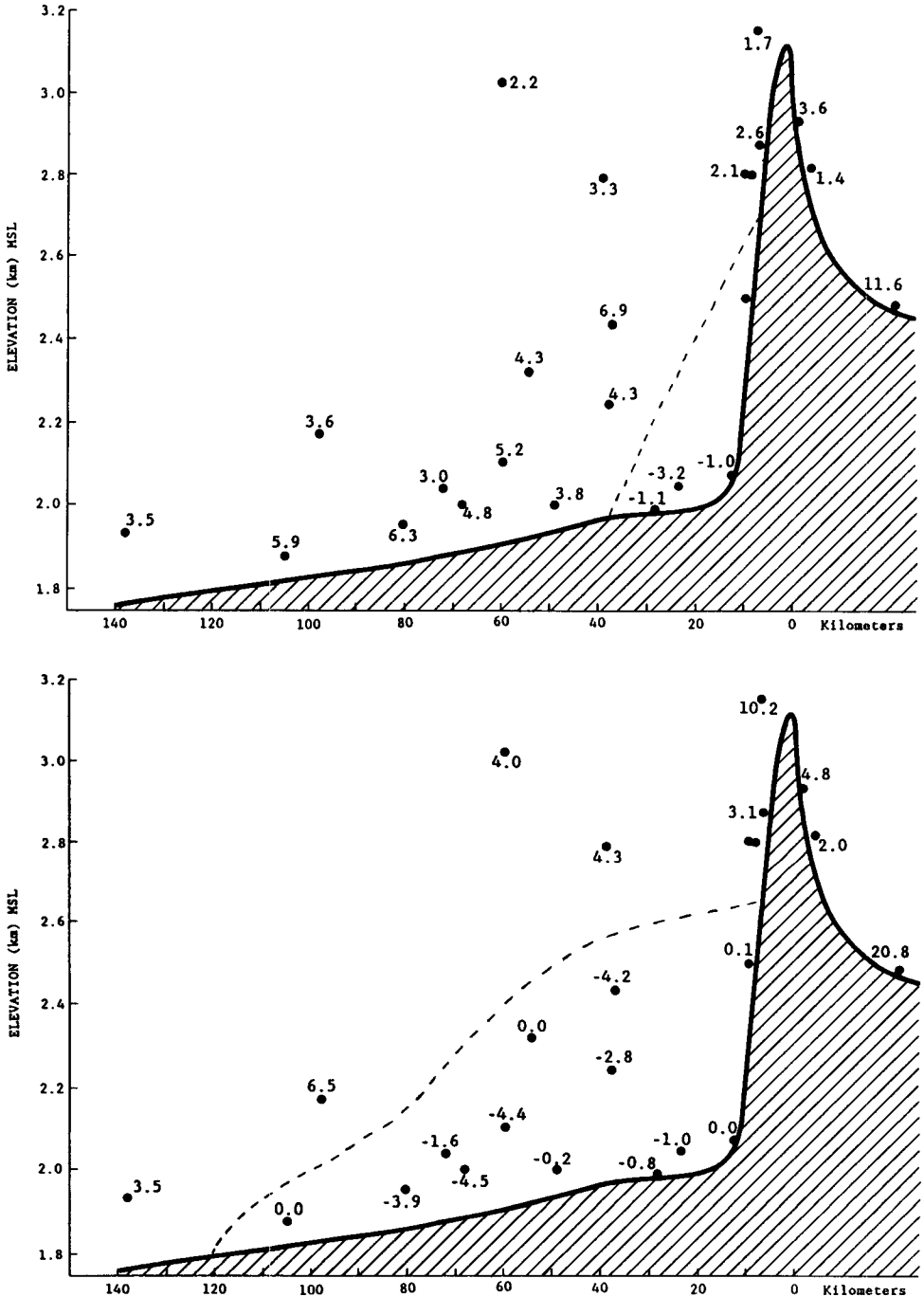

FIG. 9. (a) U wind component from the PROBE stations plotted on a generalized west–east cross section of the research area that follows the Yampa River, 1930 UTC 16 January 1982. The dashed line is the 1.5 m s^{-1} contour indicating the approximate extent of low-level decoupled flow. (b) U wind component from the PROBE stations plotted on a generalized west–east cross section of the research area that follows the Yampa River, 2245 UTC 23 January 1982. The dashed line is the 1.5 m s^{-1} contour the approximate extent of low-level decoupled flow.

rise closely corresponds to the topography with parcel rise occurring a little upwind of the rise in topography. There is a substantial rise at the barrier and many smaller rises farther to the west. The results for 23 January portray a completely different picture. The parcel rise bears little resemblance to the underlying topography. A major feature of the parcel rise trace is the decrease in parcel height at 45 km west of the Conti-

TABLE 2. Precipitation intensities averaged for 12 h on 16 January and 9 h on 23 January.

	Precipitation intensity average per station (mm h^{-1}) water equivalent	
	16 January	23 January
Total PROBE area	0.25	0.20
Over the barrier	0.74	0.35
On the barrier	0.54	0.49
Upper valley	0.33	0.30

nental Divide shown in Fig. 11b. However, this feature, which may indicate an area where the assumption of an evolving parcel is not valid, is not of prime interest to this research. The feature that is of prime interest to this research is the slightly decreasing rise 30–0 km to the west of the barrier: there is no significant increase in the lift calculated at or just upstream of the mountain barrier.

Therefore, the case study analyses indicate that when there is little or no decoupled flow, major parcel lift can be expected at the barrier. When the magnitude of decoupled flow is large and deep, primary parcel lift is not experienced at the barrier. The presence of the cloud and precipitation indicates that parcels are rising to cross the barrier, yet since the lift is not experienced at the barrier, the parcel must therefore rise farther upstream as shown in Fig. 1b.

c. *Method 3: Numerical simulations*

In an attempt to examine more closely possible correlations between the location of parcel lift and the location and depth of low-level decoupled flow, two numerical simulations of orographic clouds were performed; one with extensive low-level decoupled flow and one with little or no decoupled flow.

The model used in this analysis was the Colorado State University's Regional Atmospheric Modeling System (RAMS) (Cotton et al. 1986). It was run in a two-dimensional mode utilizing dynamics, thermodynamics, and microphysics with a horizontal grid spacing of 718 m and a vertical grid spacing increasing from 250 m near the surface to 500 m in the upper atmosphere. The domain was 215 km in the horizontal and 14.8 km in the vertical. A 5-s time step was used in the calculations. RAMS was run in a nonhydrostatic mode with a Klemp and Durran (1983) gravity wave radiation top-boundary condition. Longwave and shortwave radiation were not included in these simulations. Since the model was used to simulate the Yampa Valley and the upper Yampa Valley has very high walls that impede north–south flow, the Coriolis parameter was turned off.

The topography used was an east–west slice through the Yampa Valley from 108.76° to 106.26°W that was positioned to pass through the gap in the constricting ridges that divide the upper valley from the middle valley. This transect passed just north of Quarry Mountain. The latitude band used was 40.47°–40.49°N, which averaged three north–south 30-s resolution grid points to give a smoother slice through this rough terrain than any one pass would. This topography was then smoothed further using a Fourier bandpass filter and the ends of the domain were flattened.

A simple input sounding, shown in Table 3, was created from a composite of several soundings of winter orographic storms. The only variation in the sounding from the decoupled flow case to the no decoupled flow case was the surface temperature (though varying the surface temperature while using the same relative humidity in the sounding alters the surface absolute humidity; the surface mixing ratio is very low either way, varying from 0.25 to 0.43 g kg^{-1}). The variation in the surface temperature from −8 to −1°C was enough to change the input Froude numbers from 0.81 to 1.83, which are a little lower for the low and a little higher for the high than the case study Froude numbers of 0.94 and 1.43.

The low-level decoupled flow that developed within 2 h into the −8°C run was of sufficient strength to clearly differentiate the two runs. However, by 5 h the westward extent of decoupled flow was passing westward out of the domain. Therefore, the model was run out for 2 h dry with water only as a passive tracer followed by 2.5 h of full microphysics.

RAMS successfully modeled low-level decoupled flow from the initial conditions. However, a moderate degree of decoupled flow was not a true steady-state solution given the initial conditions and by 6 h the

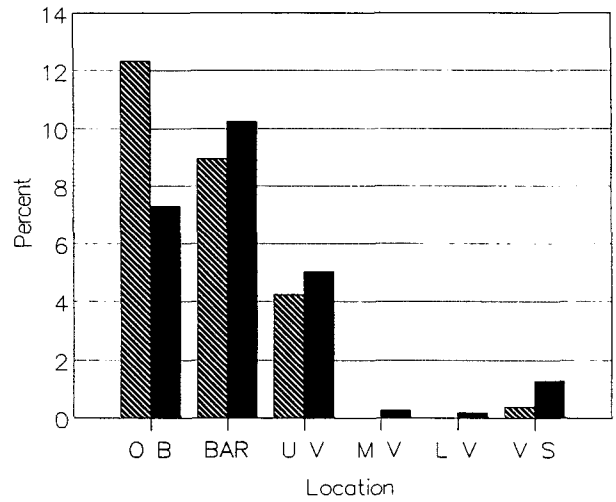

FIG. 10. Percent of precipitation by location on a per station average. Striped bar represents 16 January 1982 and the solid bar represents 23 January 1982. Locations are over-the-barrier (OB), on the barrier (B), upper valley (UV), middle valley (MV), lower valley (LV), and valley sides (VS).

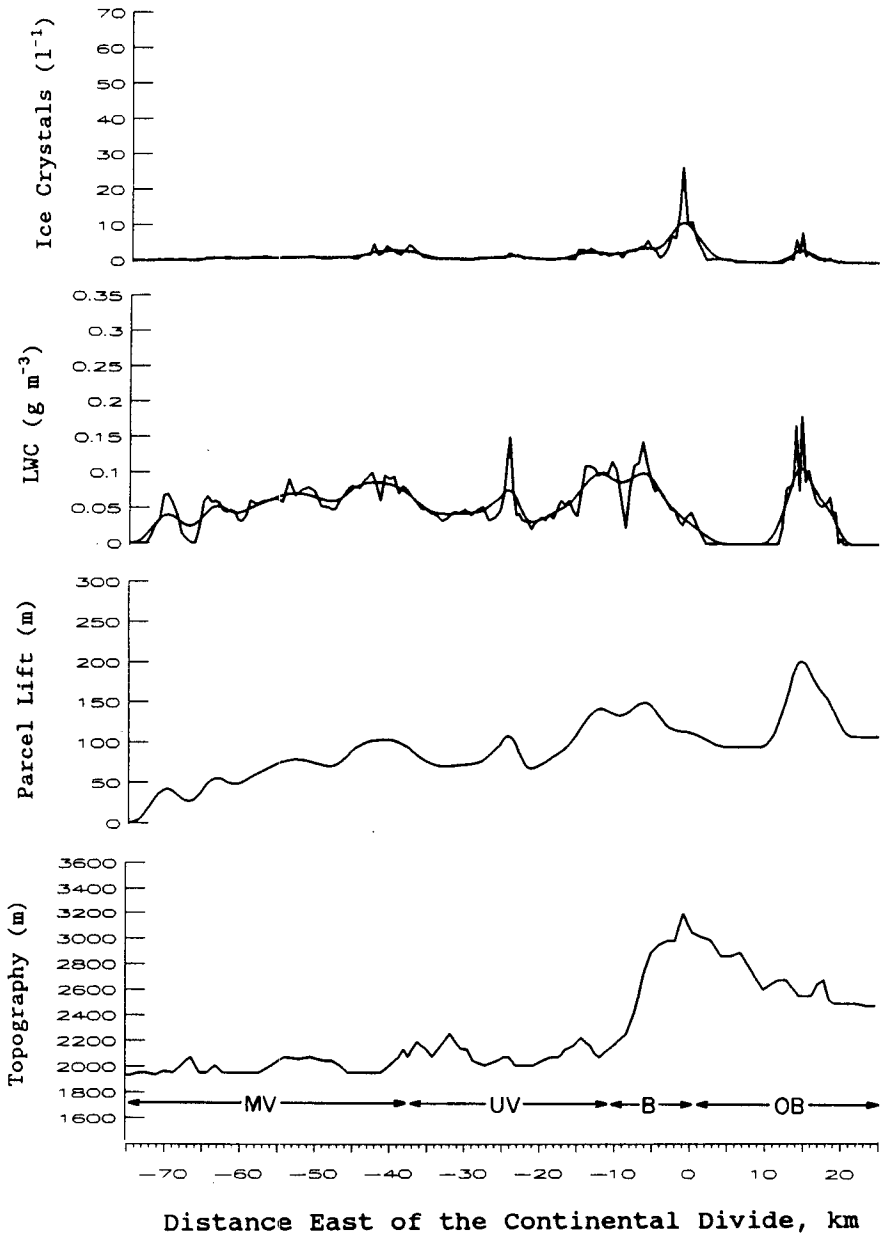

FIG. 11a. 16 January 1982 data from aircraft flight plotted along west-to-east coordinate. The top chart shows ice-crystal concentrations observed and filtered. Second from the top is cloud liquid-water content observed and filtered. Third from the top is the calculated parcel lift. Topography under the flight track is on the bottom with regions indicated for the middle valley (MV), upper valley (UV), barrier (B), and over-the-barrier (OB).

region of low-level decoupled flow had propagated west away from the base of the mountain. Figure 12 depicts the u wind at 4 h of simulation time for both the decoupled flow case (bottom) and the no decoupled flow case (top). The decoupled flow case has a 100-km region in the center of the domain with a zero or negative cross-barrier velocity. Whereas, the lowest cross-barrier wind velocity contour in the no decoupled flow case is 4 m s^{-1}.

Vertical motion fields for the two cases, shown in Fig. 13, exhibit significant differences. In the no decoupled flow case, strong vertical velocities are experienced just upwind of the barrier crest, while over the valley, there is very little vertical motion. In contrast, the decoupled flow case has a small region of moderate vertical motion just upwind of the barrier crest and a very large region of weak vertical velocity over the lower valley.

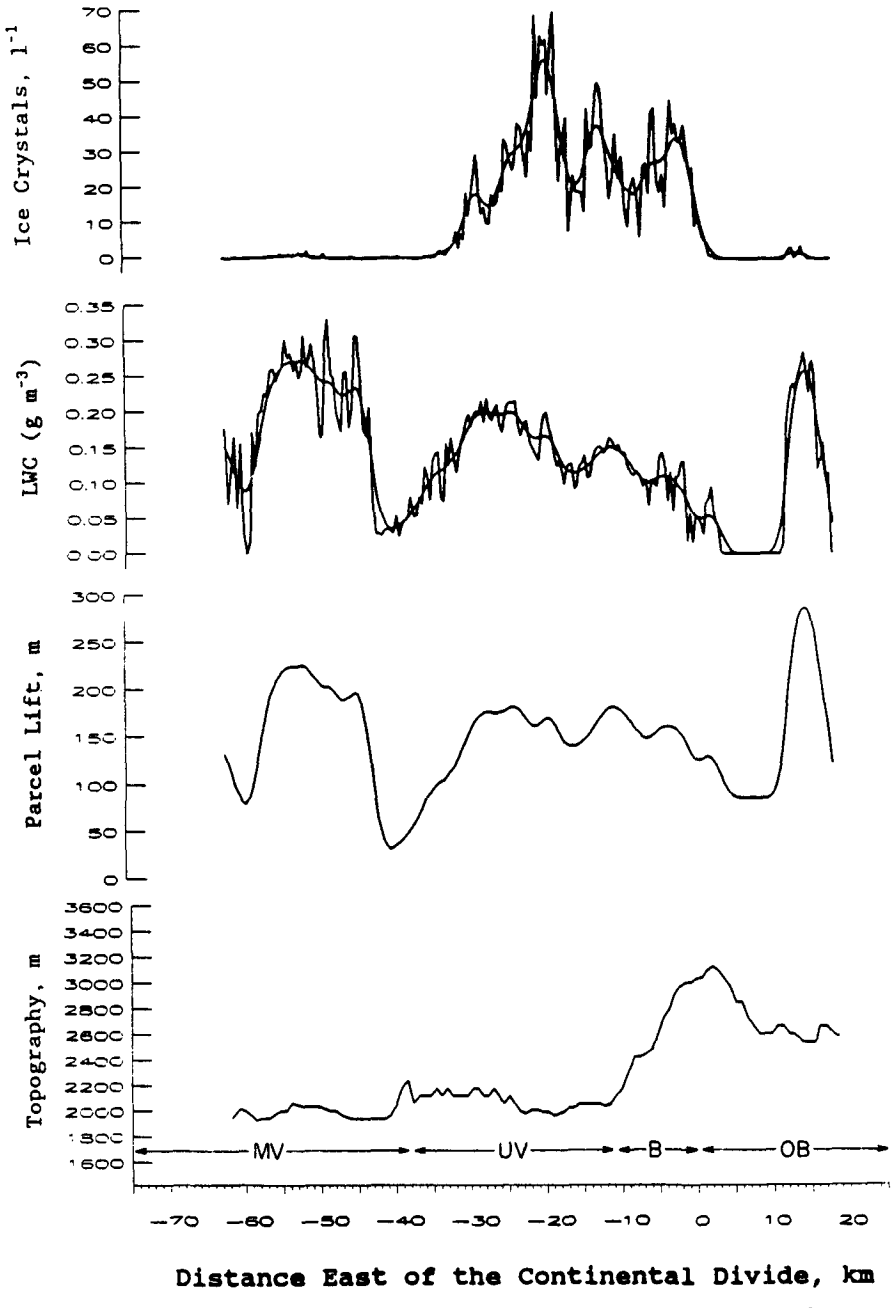

FIG. 11b. 23 January 1982 data from aircraft flight. See Fig. 8a for explanation of data.

Differences in vertical motion fields will naturally create differences in the orographic clouds formed. Within 1 h after the microphysics were turned on, both clouds had completely glaciated. Therefore, to visually depict the differences in the two cloud fields, Fig. 14 shows the cloud liquid water at 2 h. Up to 2 h, cloud liquid water accumulated as a passive tracer, it could not precipitate out and no ice could form. The clouds depicted in Fig. 14 show that the 0.08 and 0.16 g kg^{-1}

TABLE 3. Input soundings for model runs.

Pressure (hPa)	Temperature (°C)	Relative humidity (%)	Speed (m s^{-1})	Direction (°)•
70	−65	10	40	325
400	−28	10	35	310
542	−17	95	25	290
710	−11	98	15	270
825	−8 or −1	10	8	240

contours are farther upstream for the decoupled flow case than the no decoupled flow case. By 2 h the clouds are different and as time progressed, the upwind extent of the clouds increased.

Differences in clouds can lead to differences in precipitation. Figure 15 shows the total precipitation accumulation after 2.5 h of microphysics. Two significant features are readily apparent from Fig. 15. The first is the large increase in precipitation 20–80 km upwind of the barrier in the decoupled flow case compared to the no decoupled flow case. Precipitation 60 km upwind of the barrier in the decoupled flow case is twice that of the no decoupled flow case. The second feature is the overall increase in precipitation in the decoupled flow case compared to the no decoupled flow case. Only a small area over the barrier had more precipitation in the no decoupled flow case than the decoupled flow case.

5. Comparison of results from the three methods

The climatological analysis indicated that precipitation shifted upstream when the magnitude of low-

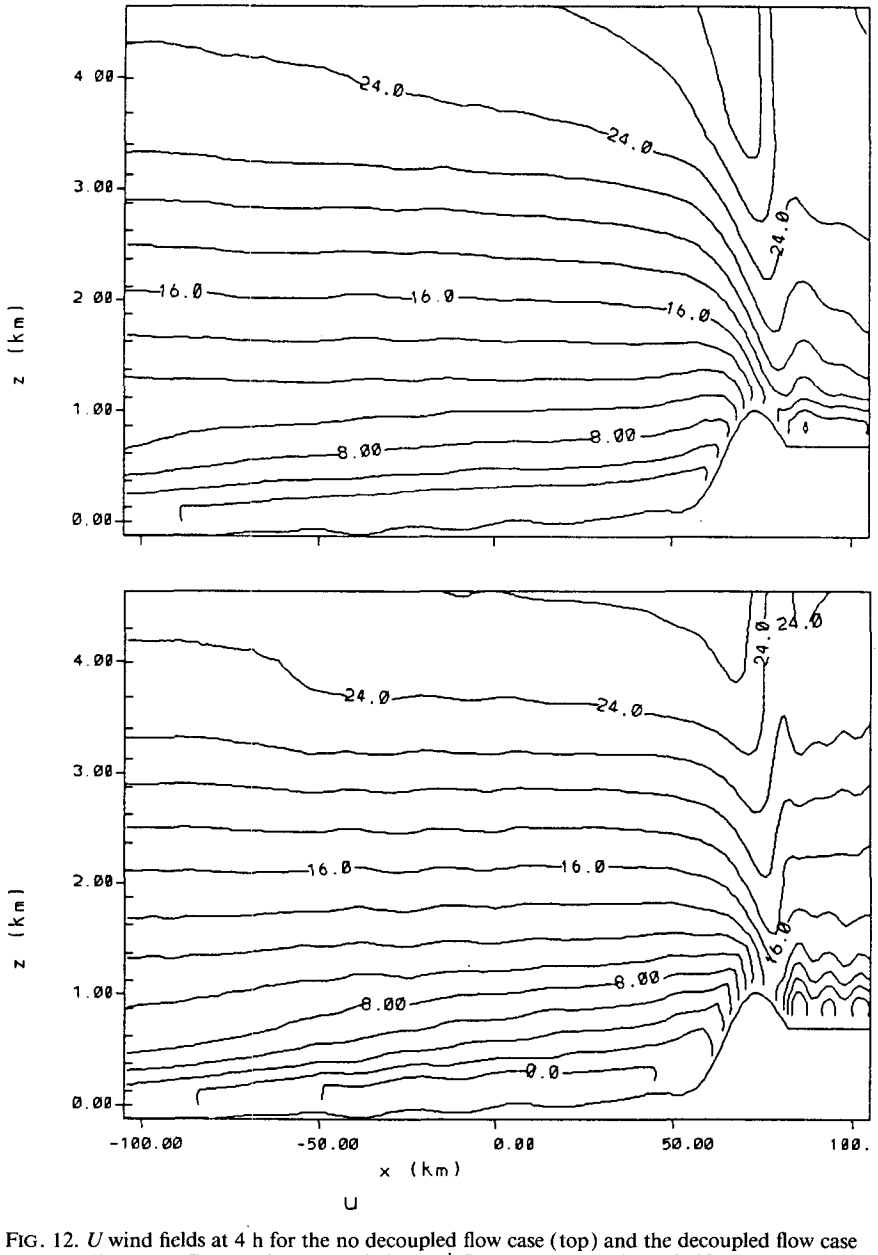

FIG. 12. U wind fields at 4 h for the no decoupled flow case (top) and the decoupled flow case (bottom). Contour increment is 2 m s^{-1}. Pressure at elevation 0 is 825 hPa.

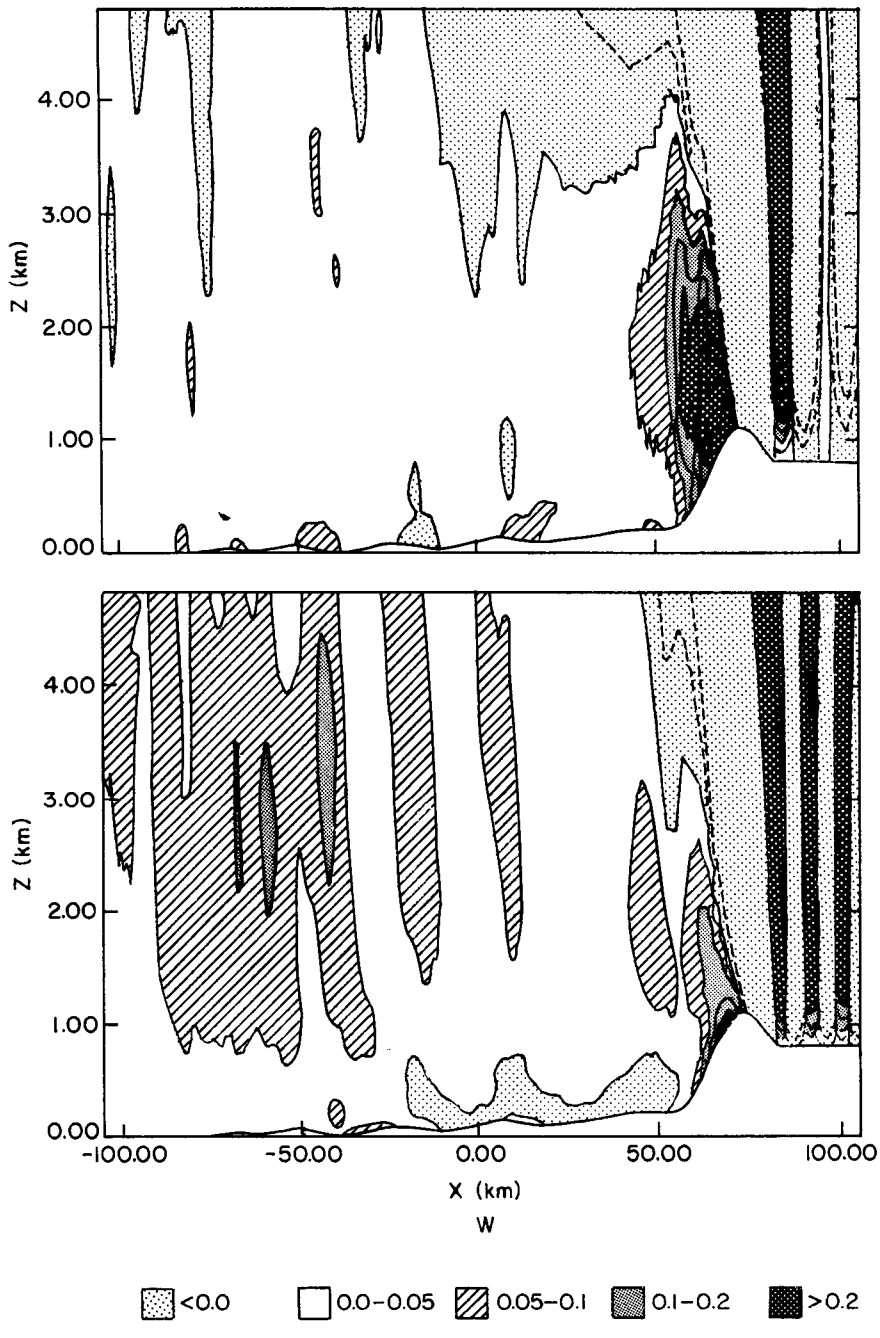

FIG. 13. Vertical wind field at 4 h for both the no decoupled flow case (top) and the decoupled flow case (bottom) in meters per second (m s^{-1}).

level decoupled flow was large. This observation was supported by the precipitation analysis in the case studies and by the numerical simulation.

In the climatological analysis, the length of blocked flow was related to the Froude number, which in turn is related to the cross-barrier wind speed. The higher the cross-barrier wind velocity, the higher the Froude number, and the smaller the blocked flow. The change in precipitation location found in the climatological analysis could not be proven to be related to differing locations of lift or simply related to different cross-barrier wind velocities, with stronger winds blowing the crystals farther east. The case studies shed some light on this question since the case with little decoupled flow also had weaker cross-barrier winds. Precipitation falling farther east on 16 January indicates that the changes in precipitation location with changes in extent of decoupled flow is not necessarily related to the

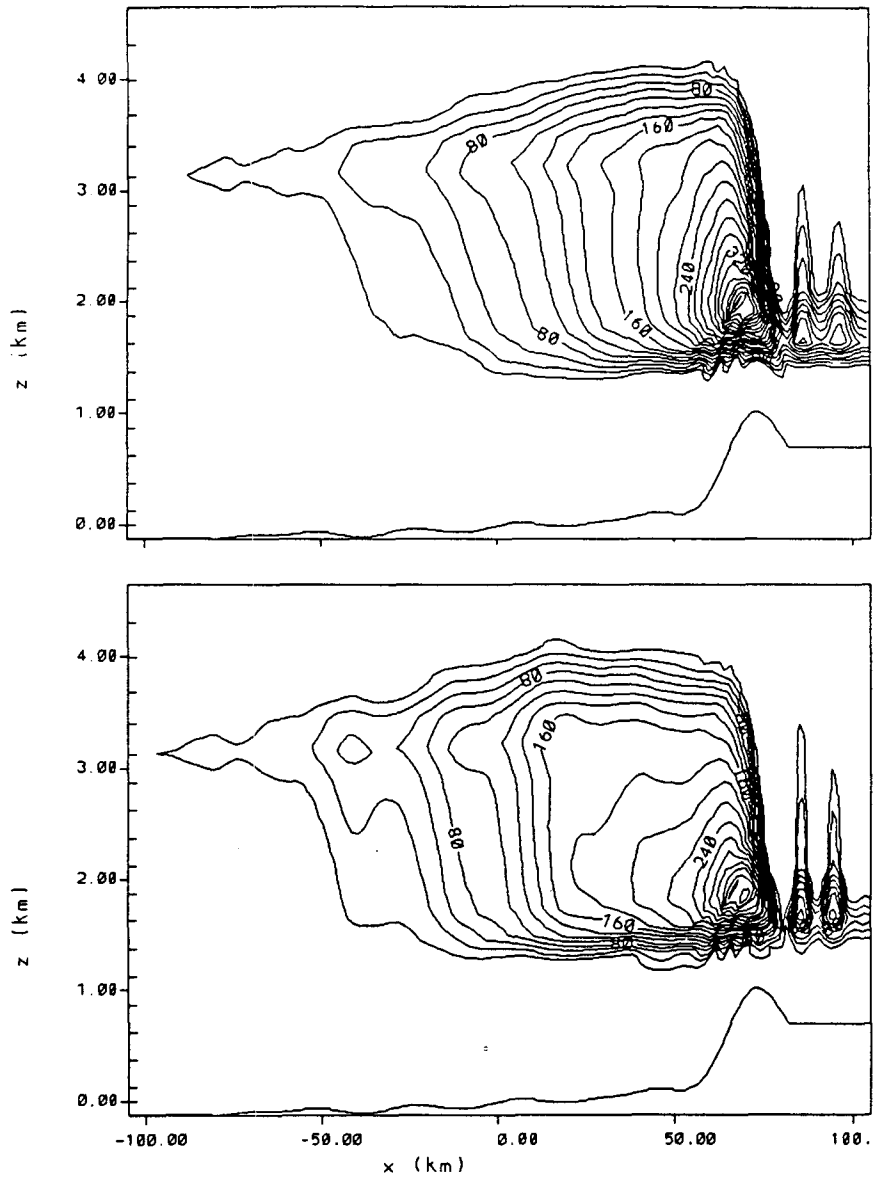

FIG. 14. Cloud liquid water at 2 h for both the no decoupled flow case (top) and the decoupled flow case (bottom). Microphysics and precipitation had not been turned on. (Units are 10^{-3} g kg^{-1}.)

strength of cross-barrier winds affecting crystal trajectories. It must, therefore, be related to changes in the location of lift and associated condensate production.

The 23 January parcel lift analysis indicates that with decoupled flow, parcels rise farther to the west. With a deep and extensive layer of decoupled flow, the location of parcel rise is not associated directly with underlying topography. The location of regions of calculated parcel lift 25–65 km west of the barrier, however, do not appear to be directly related to lift over regions of decoupled flow depicted in the cross section in Fig. 11b, either. So conclusive evidence that the parcel is indeed experiencing lift as it passes over the leading edge of the decoupled flow is not available from these case studies.

However, the results of the numerical simulation do indicate that significant lift occurs above the upwind edge of a region of decoupled flow using 0–2 m s^{-1} surface observations as a cutoff value for the definition of low-level decoupled flow. This lift, though, is not confined to a small area as if the region of low-level decoupled flow was a solid extension of the mountain. Instead it is a large, diffuse area as the oncoming flow decelerates, converges, and is forced to rise.

Another significant feature of the model output is the increase in precipitation in the decoupled flow case

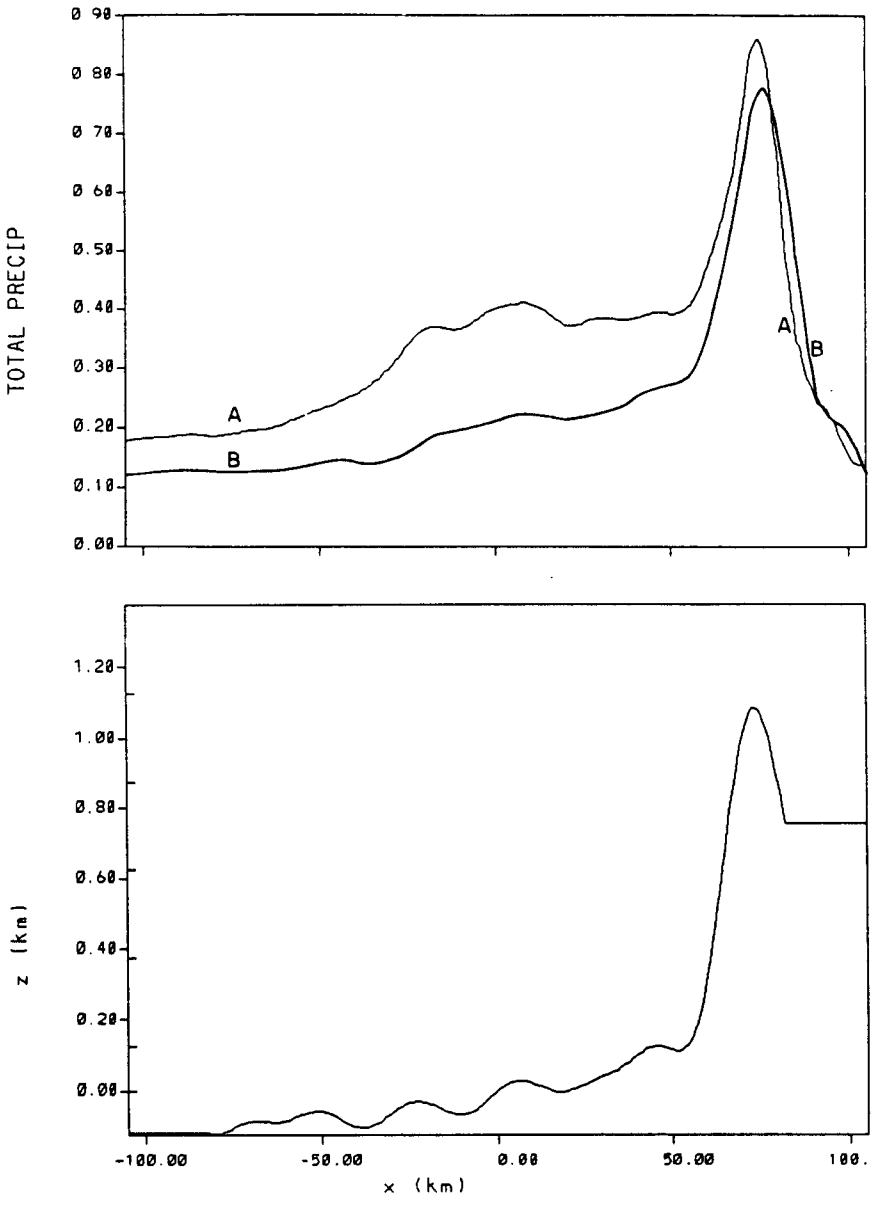

FIG. 15. Total precipitation (top) at 4.5 h (2.5 h of full microphysics) for both the decoupled flow case (A) and the no decoupled flow case (B) in centimeters (cm) water equivalence. The bottom chart is the topography.

over the no decoupled flow case. Since barrier height, cloud-level winds, and moisture were the same for both cases, the increase in precipitation was caused by an increase in precipitation efficiency. If the presence of low-level decoupled flow moved the location of condensate production farther upstream it could increase the precipitation efficiency by increasing the time available for particle growth.

6. Conclusions

The working hypothesis that low-level decoupled flow acts as an extension of the mountain for purposes of orographic lift was strongly supported by this study. In addition we found that low-level blocked flow creates more diffuse lift than the lift created by a solid mountain. Parcels of air moving towards the mountain will first have to rise over the layer of denser low-level decoupled flow before it rises over the mountain. An extended area of low-level decoupled flow upwind of the barrier will therefore cause parcel lift well upstream of the barrier, which in turn causes condensate formation farther upstream from the barrier than would otherwise occur. This change in location of condensate formation tends to shift precipitation upstream.

The shift in location of condensate formation increases precipitation efficiency, presumably because it gives ice crystals a longer trajectory in which to grow. Therefore the length of decoupled flow could be an important criterion in forecasting mountain/valley precipitation and in designing seeding experiments and evaluating their results.

Acknowledgments. The authors wish to acknowledge the assistance of Lucy McCall in drafting some of the figures and the assistance with RAMS provided by Michael P. Myers, Robert Walko, and Craig Tremback. Funding for this research was provided by National Science Foundation Grants ATM-8109590, ATM-8704776, and ATM-8813345; the Army Research Office under Contract DAALO3-86-k-0175; and the Colorado Agricultural Experiment Station Projects Colo. 113 and 692. The assistance of the Bureau of Reclamation in providing the PROBE stations for this study is gratefully acknowledged. Computations were performed at the National Center for Atmospheric Research. NCAR is supported by the National Science Foundation.

REFERENCES

Cerni, T. A., 1983: Determination of the size and concentration of cloud drops with an FSSP. *J. Climate Appl. Meteor.*, **22,** 1346–1355.

Cotton, W. R., G. J. Tripoli, R. M. Rauber and E. A. Mulvihill, 1986: Numerical simulation of the effects of varying ice crystal nucleation rates and aggregation processes on orographic snowfall. *J. Climate Appl. Meteor.*, **25,** 1658–1680.

Graw, Richard, 1990: Wintertime local circulations in northwestern Colorado. M.S. thesis Colorado State University.

Grossman, R. L., and D. R. Durran, 1984: Interaction of low-level flow with the Western Ghat Mountains and offshore convection in the summer monsoon. *Mon. Wea. Rev.*, **112,** 652–672.

Hobbs, P. V., and A. Deepak, Eds., 1981: *Clouds: their formation, optical properties, and effects.* Academic Press, 497 pp.

Klemp, J. B., and D. R. Durran, 1983: An upper-boundary condition permitting internal gravity wave radiation in numerical mesoscale models. *Mon. Wea. Rev.*, **111,** 430–444.

Lee, Robert, 1981: Wintertime cloud systems over the Colorado Rockies: Two case studies. Preprints, *Second Conference on Mountain Meterology,* Steamboat Springs, CO, Amer. Meteor. Soc., 368–360.

Marwitz, J. D., 1980: Winter storms over the San Juan Mountains. Part I: Dynamical processes. *J. Appl. Meteor.*, **19,** 913–926.

Pierrehumbert, R. T., and B. Wyman, 1985: Upstream effects of mesoscale mountains. *J. Atmos. Sci.*, **42,** 977–1003.

Rauber, R. M., 1987: Characteristics of cloud ice and precipitation during wintertime storms over the mountains of northern Colorado. *J. Climate Appl. Meteor.*, **26,** 488–524.

——, and L. O. Grant, 1982: COSE III Operation Log, Department of Atmospheric Science, Colorado State University, 444 pp.

Rogers, D. C., and G. Vali, 1987: Ice crystal production by mountain surfaces. *J. Climate Appl. Meteor.*, **26,** 1152–1168.

Smolarkiewicz, P. K., R. Rasmussen and T. L. Clark, 1988. On the dynamics of Hawaiian cloud bands: Island forcing. *J. Atmos. Sci.*, **45,** 1872–1905.